Journal of Macromolecular Science, Part A
Publication details, including instructions for authors and subscription information:
http://www.informaworld.com/smpp/title~content=t713597274

Arc-Image Testing of Ablation Materials

Edward M. Liston[a]
[a] Stanford Research Institute, California

To cite this Article Liston, Edward M.(1969) 'Arc-Image Testing of Ablation Materials', Journal of Macromolecular Science, Part A, 3: 4, 705 — 733
To link to this Article: DOI: 10.1080/10601326908053837
URL: http://dx.doi.org/10.1080/10601326908053837

J. MACROMOL. SCI.–CHEM., A3(4), pp. 705-733, July, 1969

Arc-Image Testing of Ablation Materials

EDWARD M. LISTON

Stanford Research Institute
Menlo Park, California

SUMMARY

An arc-image furnace has been used to evaluate polymeric ablators in a closely controlled experimental environment over wide temperature, pressure, and thermal flux ranges under conditions where gas phase reactions outside the char do not interfere with reactions occurring within the char.

INTRODUCTION

Arc-image testing is one of four major techniques that have been developed to test ablation polymers. The other three are: (1) plasma arc-jet testing, (2) thermogravimetric analyses (TGA), and (3) "alpha rod" testing, which uses a gas flame as the heat source.

The arc-image technique has several advantages over the others for studying the thermophysics and thermochemistry of pyrolyzing polymers: (a) Testing can be done in a completely inert atmosphere so that the chemical products recovered represent the polymer-char chemistry with no boundary layer perturbations; (b) the chemical products recovered are the result of heating rates and char temperatures that are much more representative of actual re-entry conditions than are TGA operating conditions; (c) the heating rates and resultant temperatures, the systems pressure, and the irradiation time can be closely controlled over very wide ranges so that the effect of individual variables can be studied; and (d) the absence of

boundary layer shear on the specimen makes it possible to study the physical behavior of the polymer-char system that is due to the intrinsic nature of the polymer.

This paper briefly discusses the experiments and procedures used in an arc-image facility along with representative examples of the type of data that can be obtained. These data are discussed to bring out the major findings of the program, but no attempt is made to present a complete picture of any one material system.

EXPERIMENTAL

Equipment

Figure 1 is a schematic diagram of the arc-image pyrolysis apparatus developed for use in this program. In this apparatus the light from an electric arc was focused onto the front surface of the polymer being tested by two elliptical mirrors. The sample was held in a movable sample holder which also held a calorimeter to measure the flux before and after sample exposure.

The gases given off by the polymer during pyrolysis were sampled and transferred to temporary storage flasks by a mercury diffusion pump. The use of three separate storage flasks allowed three sequential gas samples to be taken during each run. The sequence of sample acquisition was controlled by a series of electric timers that controlled the operation of the entire apparatus during the run. After completion of the run, the gas sample was transferred to small flasks that were used to transport the sample to a mass spectrometer installation for analysis.

Figure 2 is a photograph of the apparatus as installed at the Ames Research Center at Moffett Field, California. This equipment is capable of operating at flux levels from 5 to 200 cal/cm^2-sec. Tests were performed in a purified helium atmosphere with the helium acting as a sweep gas to remove the pyrolysis gases from the front surface of the char. At the helium flow normally used during these tests, it was possible to operate from 100 μ to 1 atm pressure. Most of the testing was performed between 100 μ and 1 Torr because at higher pressures the polymers gave off excessive smoke which obscured the imaged radiation. Duration of the runs was from 10 sec to 2 min.

Instrumentation

The apparatus was set up so that it was possible to measure the

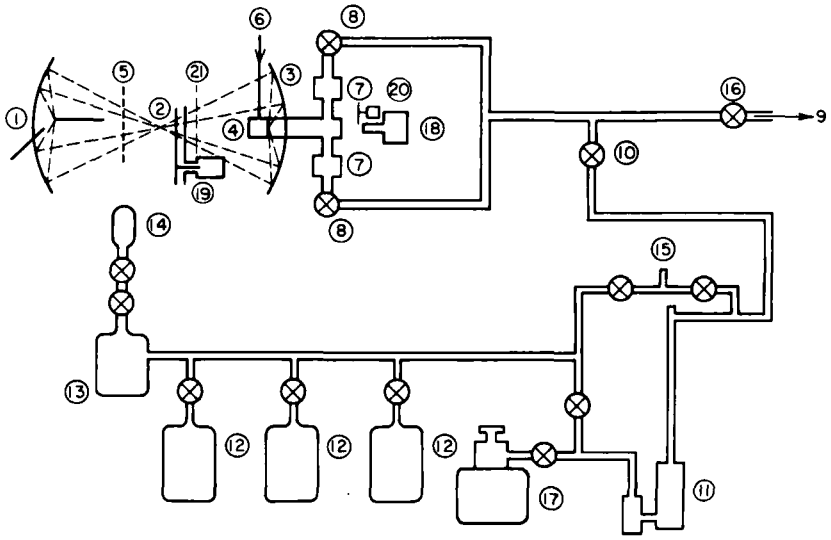

1 Primary elliptical mirror
2 Optical crossover point
3 Reimaging mirror
4 Sample holder
5 Flux moderating screen
6 Helium sweep gas inlet
7 Particulate traps
8 Sequencing valves for particulate traps
9 Gas outlet to vacuum pump
10 Sequencing valve for vapor sampling system
11 Mercury diffusion pump
12 Stainless steel storage flasks
13 Automatic Toepler pump
14 Glass transfer flask
15 Inlet position for high pressure system
16 Main vacuum control valve
17 Laboratory-type vacuum pump
18 Radiometer
19 Rear counter-rotating shutter system
20 Front shutter system
21 Optical filters

Fig. 1. Schematic diagram of the arc-image pyrolysis apparatus.

following variables continuously during each run: the internal system pressure, the front-surface temperature of the specimen, the internal temperature of the specimen at four locations, the radiant flux before and after each run, and the time at which each gas sample was taken.

The analogue signals from all these measurements were digitized and recorded on a computer-compatible tape. A computer program was used to reduce the data and plot the results.

The radiant flux was measured using a copper slug calorimeter that was shifted into the position occupied by the specimen for a few seconds before and after exposure of the specimen.

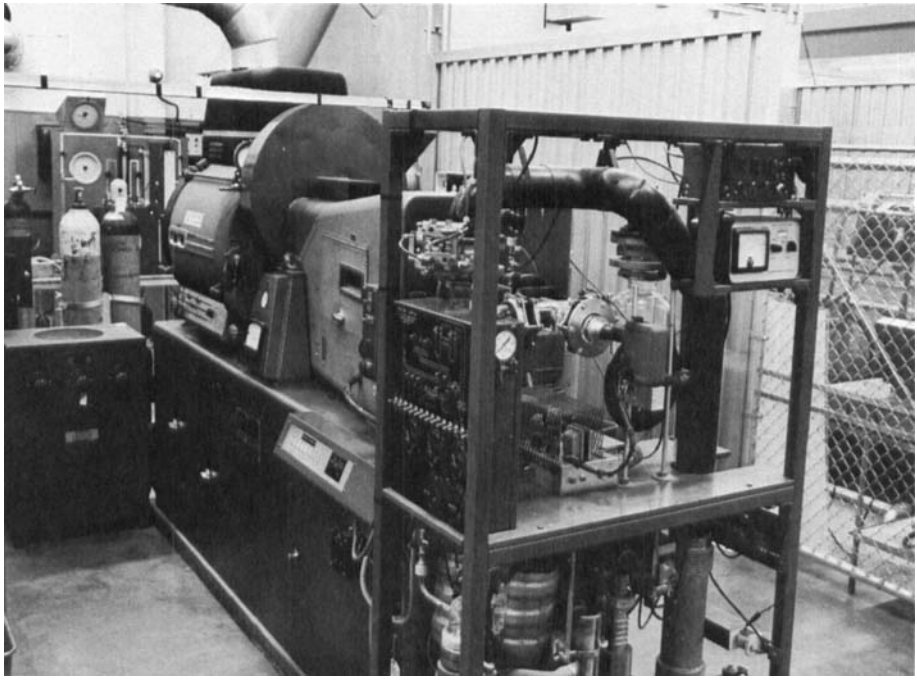

Fig. 2. Arc-image pyrolysis apparatus.

The front-surface temperature of the specimen was measured using an ultraviolet radiometer operating at 320 mμ. The ultraviolet part of the spectrum was chosen because this allows much greater accuracy of temperature measurement under the conditions that existed in the apparatus during the runs. The radiometer developed for use in this program had a response time of approximately 50 μsec. It was possible to use this radiometer to measure the cooling rate of the front surface of the specimen when the arc-image light was interrupted. This cooling rate is extremely rapid, being from 25 to 250°C/msec, depending on the polymer system.

Sample Fabrication

Samples of the following polymers were fabricated and tested during this program: (a) low-density phenolic-nylon, (b) high-density phenolic-nylon, (c) low-density polybenzimidizole, (d) DEN-438 (Dow Epoxy Novalac 438) as the unreinforced polymer and with 10 different reinforcement-filler combinations, (e) quartz-fiber-reinforced cresyl glycidyl

ether derivative of DEN-438, and (f) quartz-fiber-reinforced tertiary butyl derivative of DEN-438.

Figure 3 shows the steps for the fabrication of the samples used in this study. The samples were mounted on modified 9-pin miniature radio tube sockets (1). The tube socket was stripped of its metal base, the pins were cut down, and the base was machined so that it was just slightly larger than the specimen (2). The specimens (3) were cylindrical in shape, 1.27 cm in diam and 1.27 cm high (0.5 in. X 0.5 in.). They were drilled in such a way that thermocouples could be placed in four separate holes, which were perpendicular to the longitudinal axis of the specimen (4). These holes were drilled so that the thermocouple bead could be pulled up against a shoulder at the center line of the specimen. When the thermocouples were inserted into the body of the polymer, they were "potted" with alumina slip. This alumina slip held the thermocouple in place and also provided an electrical insulation of the bare thermocouple wire from the char. However, because of the shoulder that was machined into the hole, the thermocouple bead itself was in very good thermal contact with the char. The thermocouples were tungsten-rhenium or Chromel-Alumel and were 0.125 mm in diam. After the thermocouples were potted and the specimen was mounted on the base, the thermocouple leads were soldered to the socket pins (5). In order to prevent radial "weeping" of partially pyrolized mateial from the specimen, the edge of the specimen was coated with Saureisen cement (6).

Internal Sample Temperature

The temperature of the sample was measured at four different locations within the model. A typical plot of the temperature data is shown in Fig. 4 as produced by the automatic plotter connected to the computer. It shows the extremely rapid temperature rise within the specimen as a function of time. The rate of temperature rise decreases within the pyrolyzing specimen because the char acts as a thermal insulator for the reaction zone. The data shown in this figure were obtained from two different types of thermocouples. Thermocouples 1 and 2 were tungsten-rhenium and had a melting point of approximately 2400°C. Thermocouples 3 and 4 were Chromel-Alumel and had a melting point of approximately 1300°C.

The decrease in temperature from the maximum reading and subsequent erratic temperature measurements shown by thermocouples 1 and 2 were probably due to the failure of the alumina insulation around each thermocouple. This material reacts rapidly with carbon above approximately

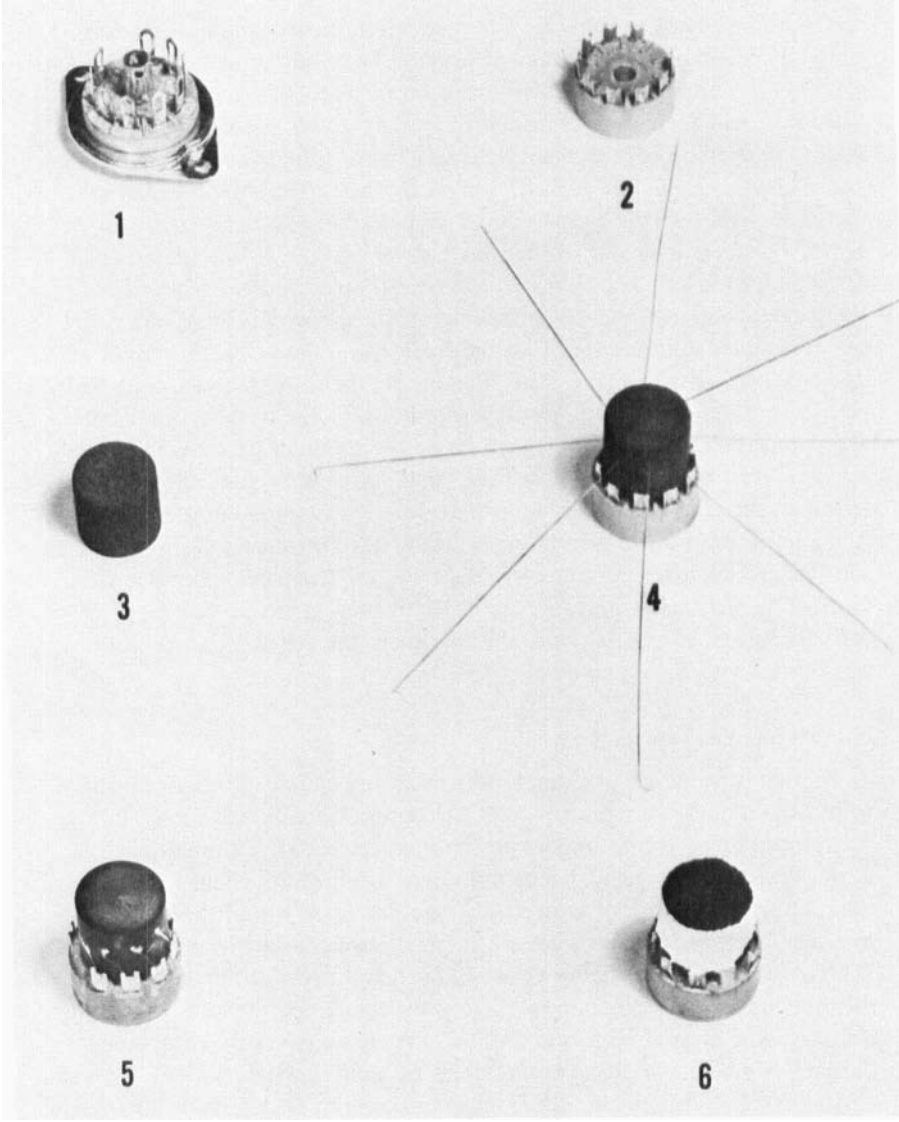

Fig. 3. Sample fabrication steps.

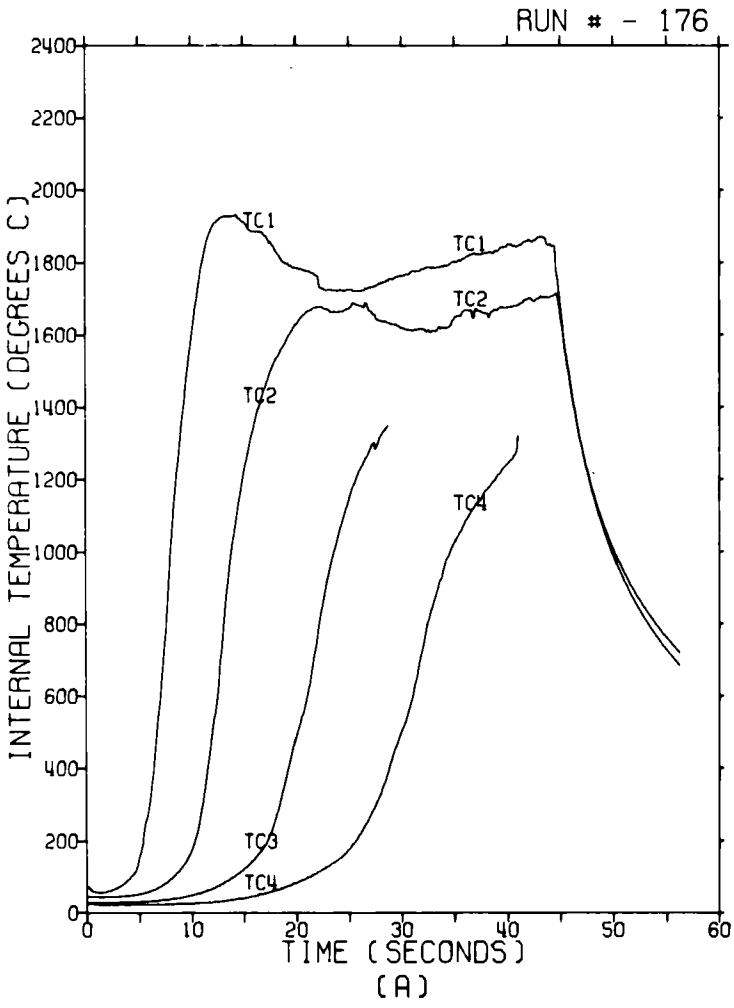

Fig. 4. Typical computer plot of internal temperature data vs. time.

1600°C. The reaction would tend to remove the alumina insulation from around the wire and cause a progressive shorting of the wire toward the edge of the specimen. As a result of this insulation failure, no reliable data above approximately 1600°C were obtained within the chars.

In order to be able to extract all of the usable information from the temperature data obtained during the runs, it was desired to cross-plot the data

to obtain plots of distance vs. time at constant temperature (the position of isotherms) and temperature vs. distance at constant time (the spatial temperature distribution within the specimen). Before this could be done it was necessary to have a mathematical model that could be used for interpolation. The model chosen was the differential equation for transient heat conduction [1] for the boundary conditions of constant front-surface temperature and constant initial internal temperature;

$$\frac{T}{T_0} = 1 - \text{erf}\ \frac{X}{2\sqrt{\alpha\theta}} \tag{1}$$

where T is the internal temperature at the point of interest, T_0 is the front-surface temperature, X is the distance from the front surface of the specimen, α is the pseudothermal diffusivity of the specimen between T and T_0, and θ is the time that has elapsed since the beginning of the run. This can be rearranged to

$$\frac{X}{\sqrt{\theta}} = 2\sqrt{\alpha}\ \text{erf}^{-1}\left[1 - \frac{T}{T_0}\right] \tag{2}$$

In order to use this equation for interpolation, it was necessary to solve for the α values at known data points from the thermocouple data and then use numerical interpolation among these data.

It should be pointed out that the α value determined from this type of calculation is not the classical α that is a conduction property of a material; rather, it is a pseudothermal diffusivity that includes the effects of conduction, chemical reactions within the char, and, most important, radiation within the char. The value determined is the average value between the front surface and the internal isotherm for which the thermal diffusivity is being calculated.

An examination of the cross-plots showed that the temperature distribution within the body was not of the shape that would be expected for transient conduction within a body of constant properties. Equation (2) predicts a monotonically decreasing temperature distribution for a material of constant thermal diffusivity. However, this was not the temperature distribution that was actually found.

At temperatures above approximately 700°C, the experimental temperature at a given distance from the front surface was significantly greater than predicted by Eq. (2). This suggested that under these conditions, radiation was a significant source of heat transfer within the char. This was substantiated by the fact that the pseudothermal diffusivity,

calculated by Eq. (2), was a strong function of temperature, being greater at higher temperatures.

Even though the pseudothermal diffusivity was dependent on temperature, it was still possible to use Eq. (2) to construct the "true" temperature distribution within the pyrolyzing char, if this dependency could be mathematically formulated.

The theoretical relationship that should exist between the pseudothermal diffusivity and temperature, for the case of radiant energy transfer within a body, has been studied by several investigators [2-5]. Each of these authors used a different approach to derive the relationship, but they all arrived at essentially the same form of equation:

$$\alpha = \alpha_0 + AT^3 \tag{3}$$

Because of the extreme complexity of the energy transfer processes occurring within the char and the great variability in the properties of the char, it was felt that it would be impossible to choose a valid mathematical model of the thermal diffusivity-temperature relationship on strictly theoretical grounds. For this reason, the thermal diffusivity data that were calculated using Eq. (2) and the data in Fig. 4 were analyzed using a regression analysis computer routine to see if they fit the form of Eq. (3). Figure 5 is a plot of the thermal diffusivity data as a function of temperature for one of the high-density phenolic-nylon specimens. The regression analysis of these data for thermocouple 3 gave the following results:

$$\alpha = (2.8)10^{-3} + (2.6)10^{-12}\, T_K^3 \tag{4}$$

This equation, plotted in Fig. 5, fits the experimental data between 400 and 1200°C to approximately 1.3%. The regression analysis on each of the other thermocouple data sets was just as good. These data were calculated using the nominal location of the thermocouples, and all the data should have fallen on the same line. The fact that the data from thermocouple 1 do not is due to its being slightly off its nominal location. Theoretically all the points in Fig. 5 could be corrected to fall on the same line by making small changes in the X values for which they were computed. For example, by increasing the X value for the first thermocouple by 12.9% (0.0328 cm), the α values for this position are increased by 29%, and they fall almost exactly on the other two sets of data. The correlating equation for all the data in Fig. 5, with the first thermocouple location corrected by 12.9%, is

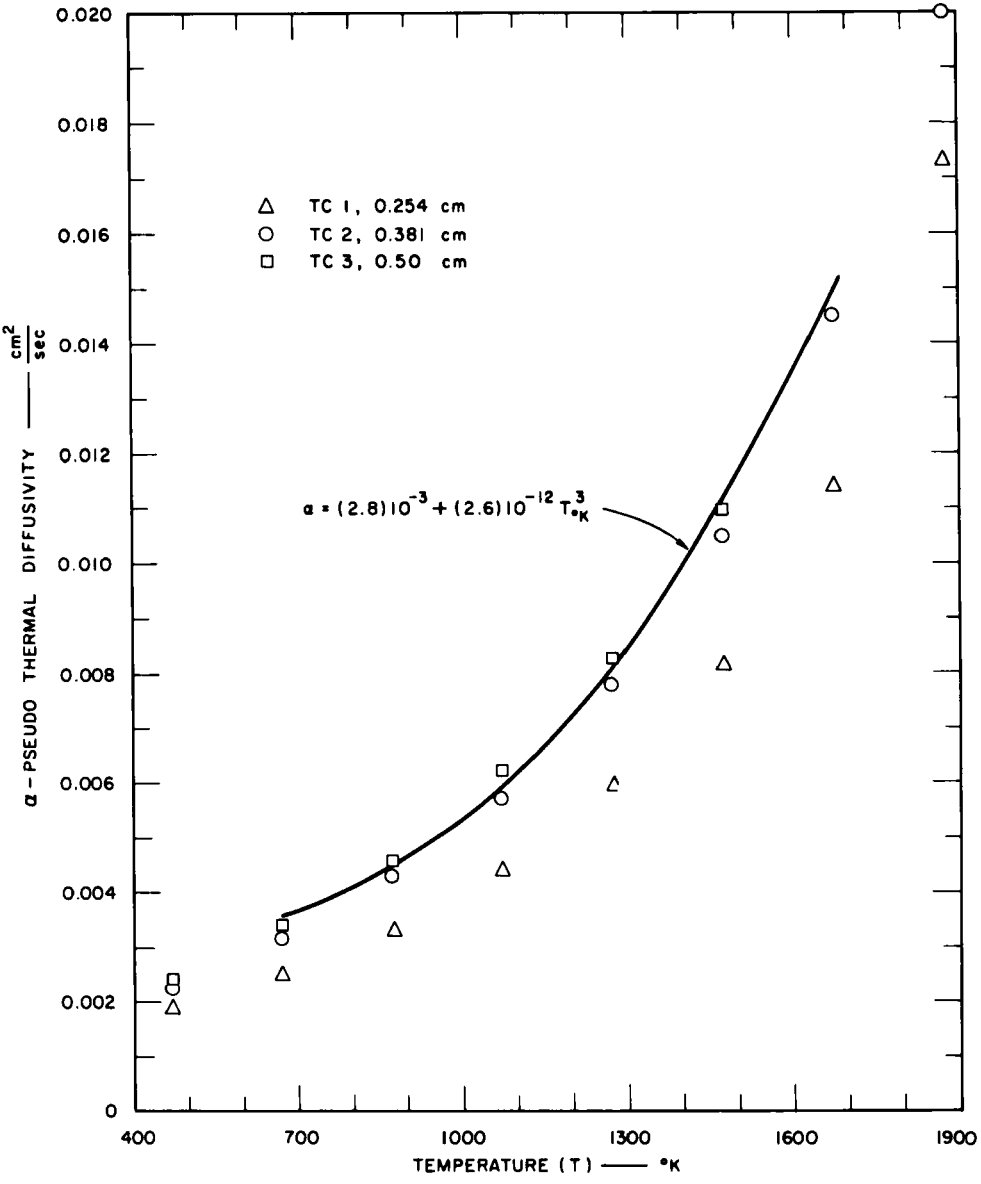

Fig. 5. Pseudothermal diffusivity vs. temperature.

$$\alpha = (2.25)10^{-3} + (2.77)10^{-12}\ T_{o_K}^{3} \qquad (5)$$

with an average error of 4.9%.

The numerical results obtained for the thermal diffusivity of chars in this program agree very well with those obtained using a special thermal conductivity test apparatus [4].

It was therefore felt that the derived relationship, Eq. (3), applies in this case and could be used for analysis of the internal temperature data.

A specific example of how it was used is shown in Fig. 6. In this figure the solution to Eq. (2), with a constant thermal diffusivity of 0.004, is shown for the conditions of θ = 25 sec, T_o = 2400°C. This curve intersects the measured temperature distribution curve for 25 sec at 500°C and correctly predicts the location of the 500°C isotherm as being at X = 0.57 cm.

If the thermal diffusivity term in Eq. (2) is replaced with a term of the form shown in Eq. (4), a curve of entirely different shape results. This curve is also shown in Fig. 6. As can be seen, the fit of the prediction using a variable thermal diffusivity is far better than that using a constant thermal diffusivity. It is unfortunate that it was impossible to obtain reliable data above 1600°C, since there is no way in which the higher-temperature part of this predicted curve can be checked with the experimental data obtained.

For the temperature range between 400 and 1200°C, the fit between the predicted curve and the experimental curve is very good in terms of distance from the front surface. However, below 400°C the curves deviate very significantly. This deviation is probably due to the fact that below 400°C the temperature is being measured in the polymer, whereas the dependence of thermal diffusivity on temperature was determined in the char.

Equation (4) was used in Fig. 6 instead of Eq. (5), because Eq. (4) was calculated from thermocouple 3 data and the prediction was being made at approximately the position of thermocouple 3 (0.5 cm).

While the correlation between the actually measured data and the predicted curve is very good for the positional data, it is not nearly as good for the temperature data. This can best be seen in Fig. 7. In this figure the solid lines are the actually measured data, while the dashed lines are extrapolations of those data using a second-order fit.

The points marked on the figure were constructed using Eq. (3) and a constant value for themal diffusivity that was determined at 800°C at the

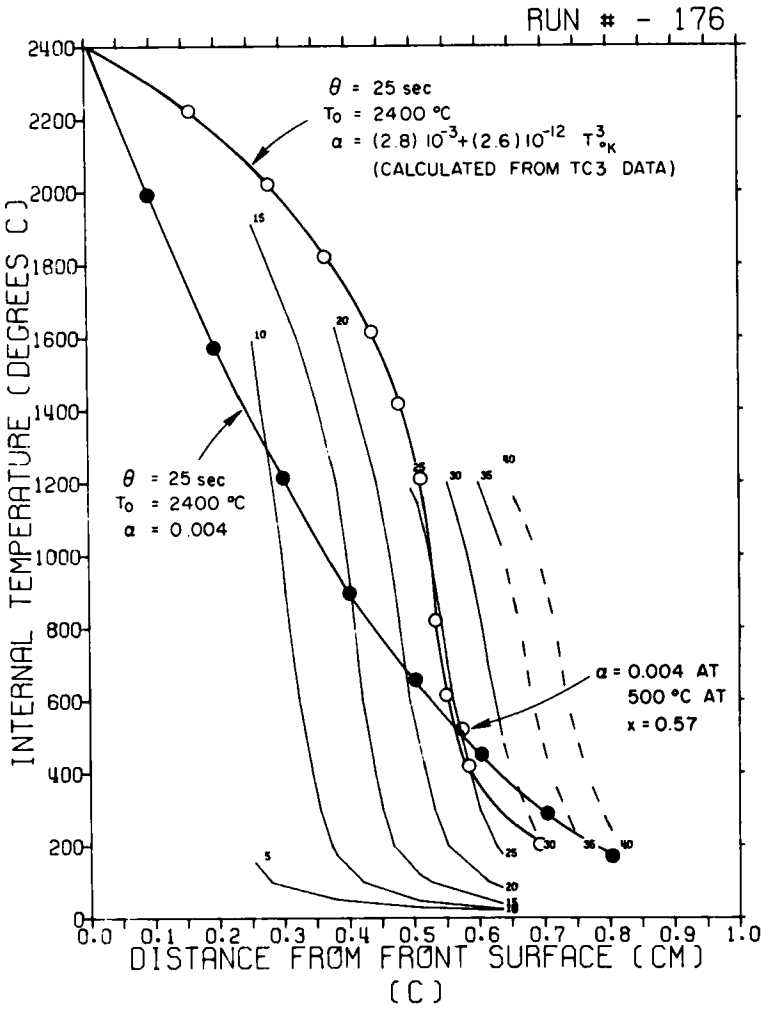

Fig. 6. The effect of variable thermal diffusivity on calculated internal temperature profiles.

position of the third thermocouple, X = 0.508 cm. It can be seen that the curve constructed from the theoretical relationship does not follow the measured curve accurately. The main reason for this is that very small errors in the measurement of X can produce very large perturbations in the value of the second derivative of temperature with respect to X.

If the "correct" value for the thermal diffusivity at 800°C and 0.7 cm from the front surface is taken from Fig. 5 and is used to calculate the position of this isotherm, the value calculated falls almost exactly on the extrapolated 800°C line in Fig. 7.

Because these variations in the thermal diffusivity due to small errors of the measurement of X are essentially a random process, no mathematical model was possible for correlating the variations.

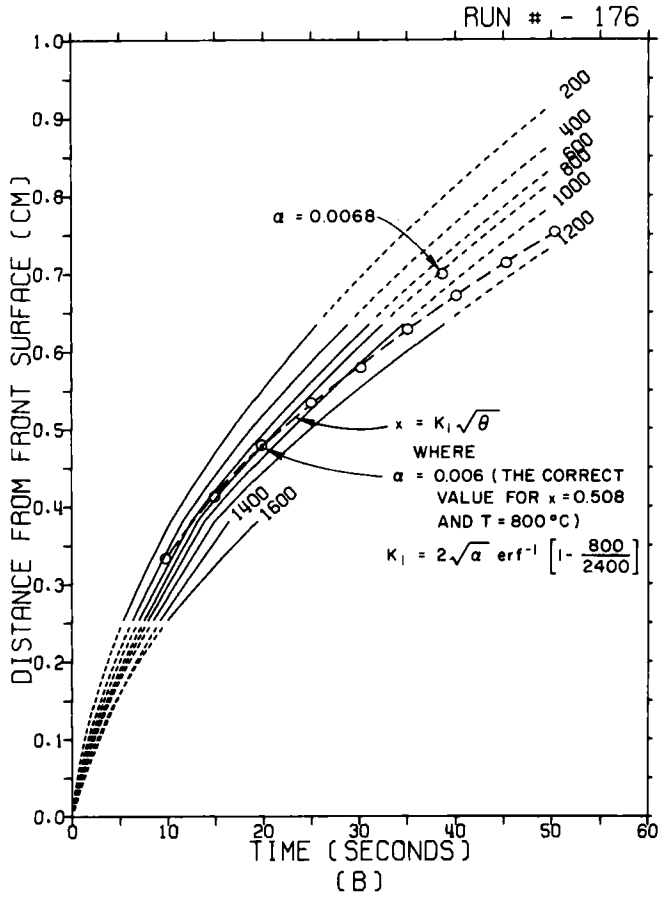

Fig. 7. Example of the prediction of isotherms.

Polymer-Char Interface Recession

As previously shown in Fig. 4, the char acts as a thermal insulator for the polymer. There are many data to show this. The first can be seen in Fig. 4, where it is obvious that the rate of temperature rise in the pyrolysis zone (600-800°C) decreases as the char thickness increases. The cross-plot of these data, Fig. 7, shows that the rate of motion of all of the isotherms slows as the char thickness increases (there is no front-surface char removal, so char thickness increases with increasing run time).

Figure 8 illustrates the same fact using gravimetric data. In this figure the "differential polymer recession rate" is the difference between the maximum polymer recession of the run in question and the next shorter run, at approximately the same flux level, divided by the difference in time between the two runs. For example, if two runs had been made at essentially the same flux and pressure conditions, one for 30 sec and the other for 45 sec, the maximum polymer recession for the 30-sec run would be subtracted from the maximum polymer recession for the 45-sec run and this difference would be divided by 15 sec. This value was calculated because it shows much more clearly than does the maximum recession rate itself the effect of increasing char thickness on the pyrolysis rate.

In this figure the curves all show that the recession rate of the polymer-char interface decreases very rapidly as the char thickness increases. This is to be expected, since the energy causing the polymer-char interface recession has to travel through the char, and as the char increases in thickness it acts as a better and better insulator of the polymer-char interface. These curves also show that any factor that will tend to decrease the char thickness will force the polymer-char interface velocity to increase. Thus, oxidative removal of char, spalling of char, or erosive removal of char will cause the polymer-char interface velocity to increase and thus will decrease the effective lifetime of the ablation heat shield. This relationship between the differential polymer recession rate and char thickness points out the necessity of developing chars with high structural strength and good physical integrity for use under high heating conditions.

Chemistry of Pyrolysis Gases

Figure 9 is a plot of the composition of the pyrolysis gases given off by low-density phenolic-nylon. It can be seen that the major component, on a mole fraction basis, is hydrogen, which increases during the run because the high-molecular-weight hydrocarbons are cracked to a progressively greater degree as the char increases in thickness. The CO increases

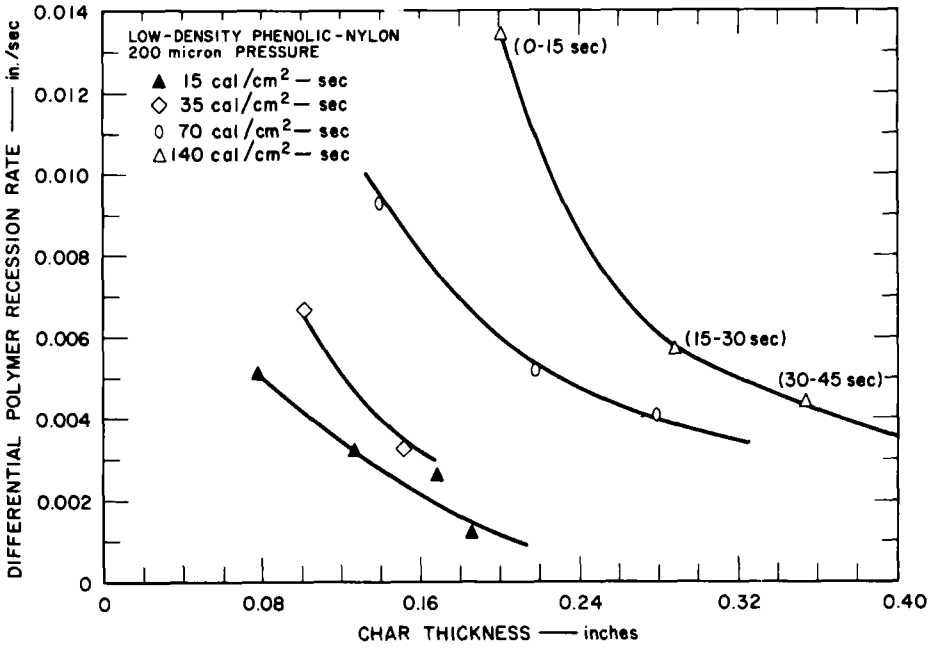

Fig. 8. Differential polymer recession rate vs. char thickness.

somewhat on a mole fraction basis as the reaction between water vapor and the hot carbon produces CO and hydrogen.

Higher-molecular-weight compounds were found in the pyrolysis gases, but they were present only in very small amounts. This was as expected for two reasons: (1) The higher-molecular-weight materials have low vapor pressures and are unable to flow from the pyrolysis area to the sample flask without being absorbed, and (2) once a hot char had formed, these gases would be cracked by the hot char to much lower molecular weight material.

Evidence for the first process was the strong odor of phenols and cresols that was always present in the apparatus after a run; these are known to be major constituents of the gases given off by the polymer during TGA testing. Evidence for the progressive cracking of the pyrolysis gases is provided by Fig. 9, which shows that all the hydrocarbon species decrease in concentration with increasing run time (increasing char thickness). Therefore, it was concluded that high-molecular-weight materials were formed but only during the initial stage of the char formation

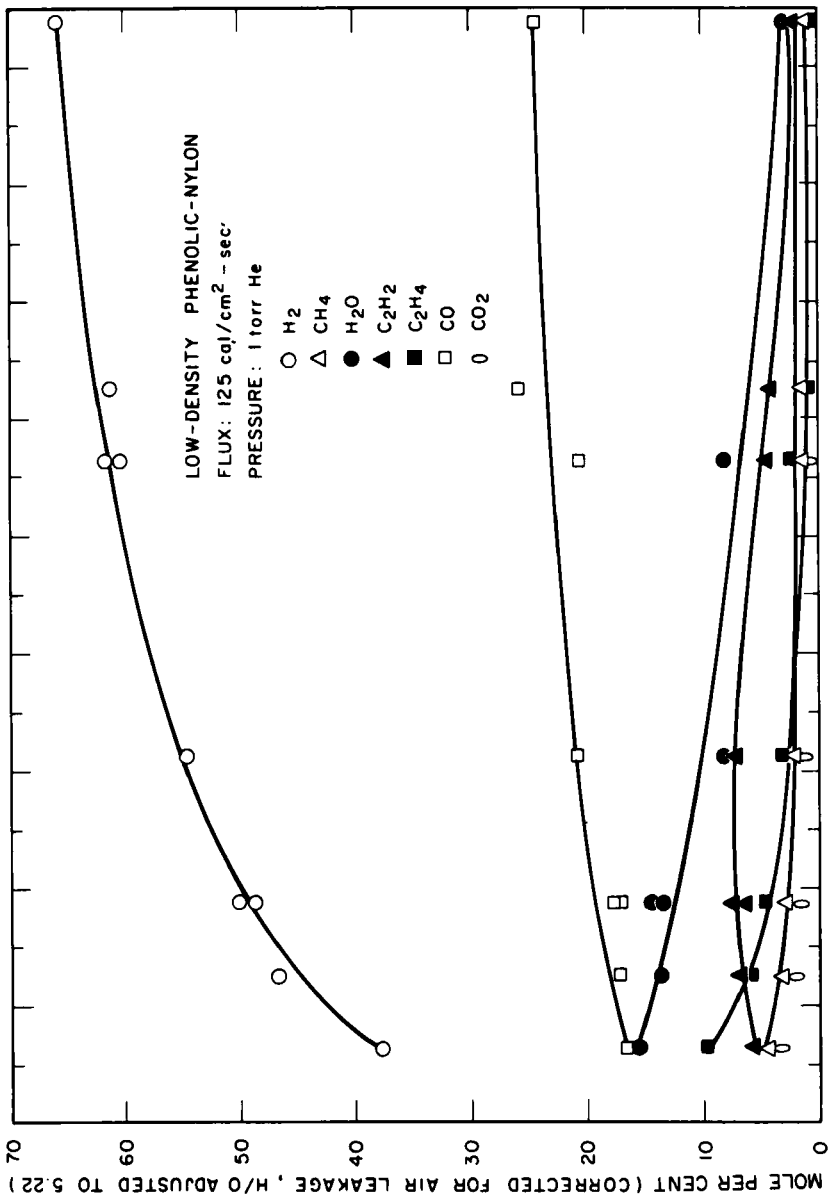

Fig. 9. Chemical composition of pyrolysis gases on a mole basis: low-density phenolic-nylon.

process before there was sufficient char to crack them. After a char had built up on the polymer, the major constituents of the pyrolysis gases were hydrogen and carbon monoxide, other components being present in very small amounts.

Char Formation Processes

As can be seen by an examination of the internal temperature data in Fig. 4, the first thermocouple showed a small rise in temperature when the sample was first exposed to the radiant flux. The rise was caused by the radiation penetrating into the body of the polymer before an opaque char had formed on the surface. From these data is can be seen that it took approximately 1 sec for the char to form. It should be stressed that it took that long even though the surface of the specimen was coated with Kodak black brushing lacquer before testing began. At much lower fluxes and without the preblacking of the surface, it took as long as 30 sec for an opaque char to form.

During this initial char formation process, the polymer lost material by three different processes: (1) the "spitting" of molten polymer in low glass-transition materials, (2) the vaporization of partially pyrolyzed polymer, and (3) the incomplete cracking of high-molecular-weight species in the thin char.

In an attempt to get more information about the properties of the char and the char initiation processes, an X-ray density-measuring apparatus was devised. This apparatus consisted of a motor-driven sample holder attached to a slightly modified commercial X-ray diffraction unit. In order to measure the X-ray density of a specimen, it was sectioned into a piece approximately 2.5 mm thick. Then the specimen was mounted in the sample holder, and it was slowly passed in front of a slit on the X-ray Geiger tube. This slit was 0.05 mm wide and therefore the resolution of the measurement was approximately 0.075 mm.

The apparatus was calibrated against chars of known density and several different polymer-filled systems. In all cases, the Beer-Lambert Law held within the experimental accuracy of the measurements. This procedure gave excellent reproducibility in measuring the "density profile" of the char. However, since the X-ray absorption coefficient of silica is about the same as that of carbon, any nonuniformity in the distribution of reinforcement had a strong influence on the observed density profile of the char. Therefore, it was not possible to obtain the true carbon density profile in any char where the silica had reacted with the carbon to form either silicon monoxide or silicon carbide.

Figure 10 shows three superimposed X-ray density profiles of chars made from a high-density epoxy-novalac with 5% chopped quartz fiber. The three chars had the following pyrolysis histories: One char had a 15-sec exposure; the second had a 30-sec exposure; and the third had a 15-sec exposure, after which the sample was removed and about half of the char was sanded off, then the sample was remounted and exposed for an additional 15 sec.

All three of these profiles show the same characteristics. There is an initial density decrease from the polymer density to a density minimum in a region approximately 0.5-0.7 mm thick. This density minimum corresponds to the weakest part of the char—the point at which the char releases from the polymer body when it is pried off. The material left on the polymer body when the char cap is removed is the material to the right of the density minimum in Fig. 10. This material corresponds to the "primary pyrolysis" zone of the polymers. The "yellow zone" is a layer of mechanically cracked polymer that shows the same X-ray density as the uncracked polymer and is to the right of the primary pyrolysis zone in Fig. 10.

The increase in density to the left of the minimum is caused by the thermal cracking or "secondary pyrolysis" of the gas products generated during the primary pyrolysis of the polymer. As these gases crack, they deposit carbon on the existing char, and there is a net carbon density increase to some peak value. In the three profiles shown, the position of this peak was at about the same relative position within the char (60% of the distance from the front of the char to the density minimum). It is therefore probably valid to assume that the position of this density maximum corresponds to essentially the same temperature within the char regardless of the char thickness.

The decrease in density between the maximum peak and the front of the char is the result of at least five competing carbon removal processes. These are: (a) carbon sublimation from the front surface of the char, (b) the reaction between water vapor and carbon to form carbon monoxide and hydrogen, (c) the reaction between carbon and hydrogen to form acetylene, (d) the reaction between carbon dioxide and carbon to form carbon monoxide, and (e) the reaction between silica and carbon to form carbon monoxide and silicon monoxide.

The run with two separate 15-sec exposures was included in this series to determine whether the density decrease toward the front of the char was occurring during the pyrolysis process or whether it was some sort of "memory" of the char initiation process. As can be seen in Fig. 10, the

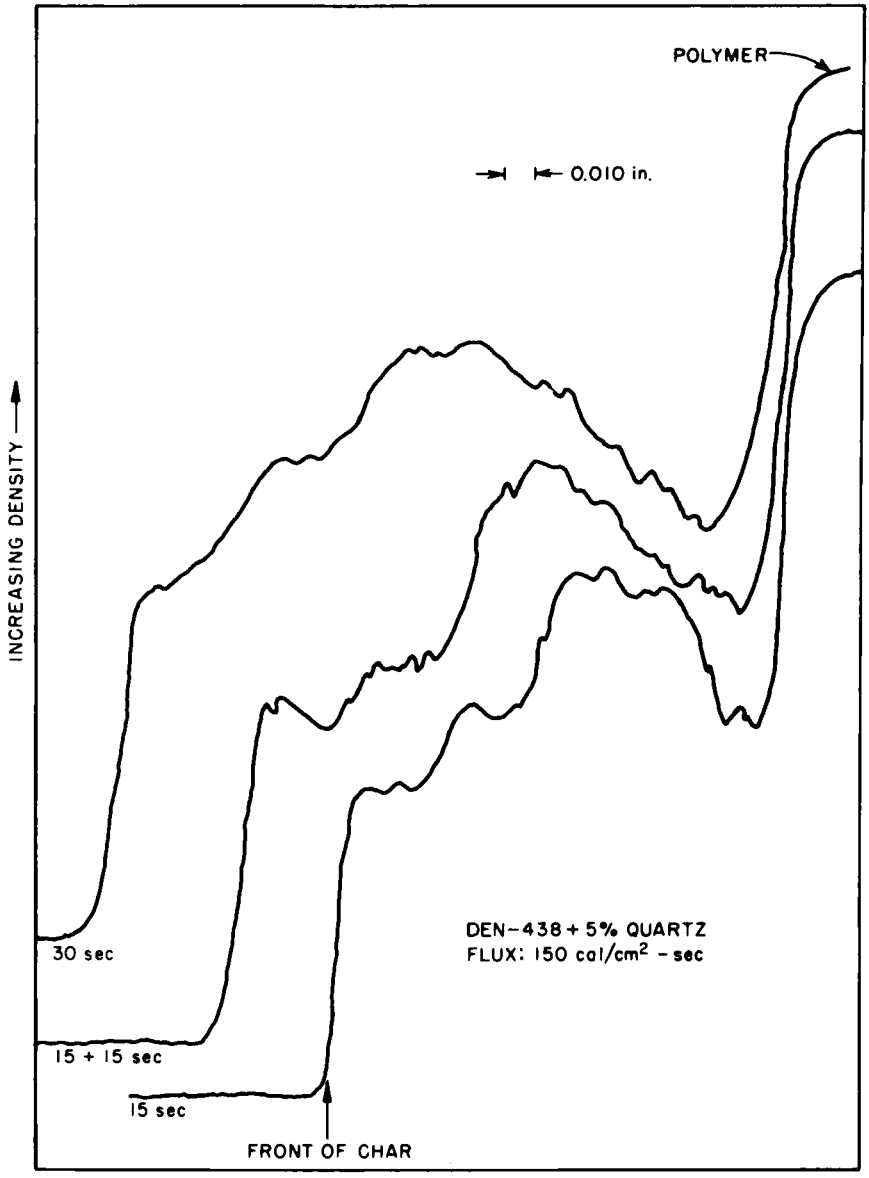

Fig. 10. X-ray density profiles.

drop in density is present whether the original char is present or not. Therefore, it was concluded that the density decrease did occur during the charring process and was not an artifact caused by the initiation processes.

Additional evidence for the location and thickness of the pyrolysis zone can be obtained from the internal temperature profiles shown in Fig. 6. It can be seen from this figure that the temperature in the pyrolyzing sample rose from approximately 300 to 1000°C in about 0.7 mm. This distance corresponds very closely to the measured thicknesses of the low-density gap in the X-ray density profiles. The temperature data therefore confirm the conclusion that the primary pyrolysis and much of the secondary pyrolysis occurred in the low-density region.

A third way in which the pyrolysis zone was located was by analysis of the char for carbon-hydrogen ratio. After the char cap was removed, approximately 0.5 mm of char remained on the polymer. This char was shaved off in two layers and each layer was analyzed for the carbon-hydrogen ratio. The material immediately adjacent to the polymer had a ratio of approximately 20:1. The next layer had a ratio of between 50:1 and 80:1. Finally, the 0.25-mm layer of char immediately to the left of the low-density region had a carbon-hydrogen ratio in excess of 100:1. These data again confirm that the pyrolysis occurred in an extremely narrow region immediately adjacent to the polymer-char interface.

The effect of secondary pyrolysis on the char yield of a polymer is shown in Fig. 11. In this figure, "gravimetric per cent char yield" is defined as the weight of char formed divided by the weight of polymer that went into forming that char. It can be seen that there is a very significant increase in char yield over that obtained in TGA testing. This increase is the result of carbon deposition from secondary pyrolysis processes and is a quantitative measurement of the density increase observed in the X-ray density profiles (Fig. 9).

Failure Processes

The physical behavior of the polymer-char systems was studied quite extensively during this program. It was found that several polymers which showed excellent potential as ablators in TGA tests had very poor thermophysical stability under the extreme heating conditions of simulated ablation testing. These studies were undertaken to find means of stabilizing the polymer-char system during high-heating-rate conditions so that the good char-forming potentialities of the polymer could be realized.

Figure 12 shows results of the catastrophic failure of an unreinforced epoxy polymer. This material showed excellent char-forming properties

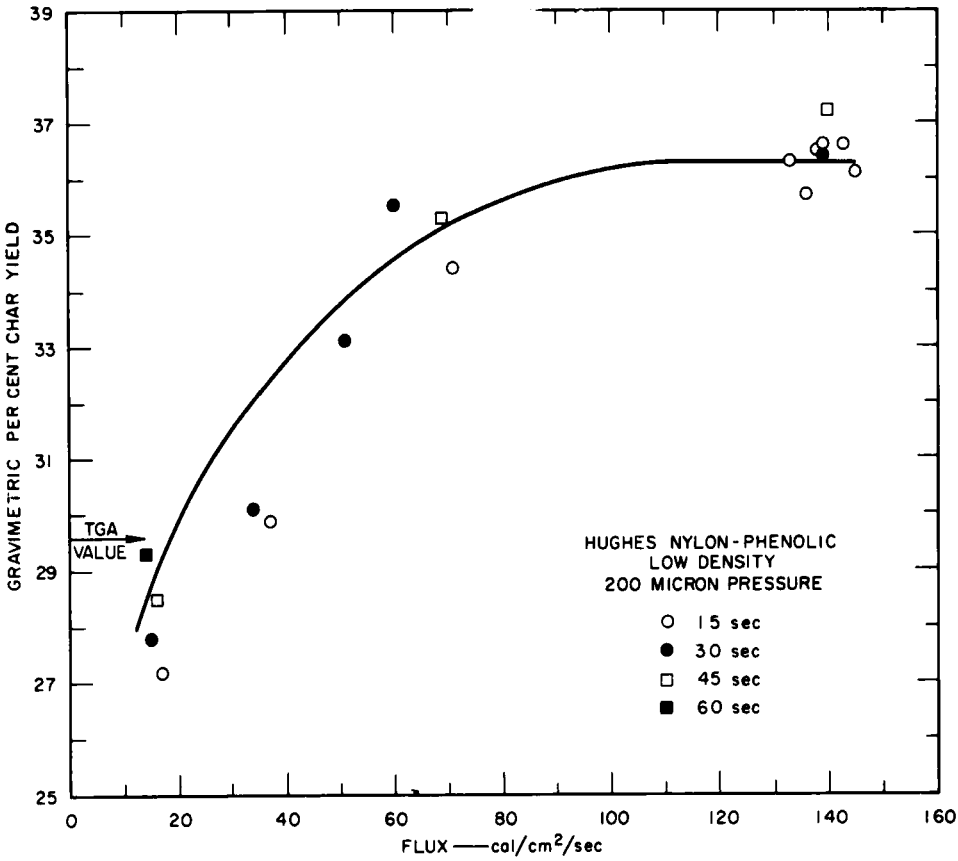

Fig. 11. Gravimetric per cent char yield vs. flux.

under TGA heating conditions. However, when the sample was tested in the arc-image facility, it began to fail immediately upon exposure to the radiant flux. The failure consisted of the spalling of small pieces of polymer from the front surface of the specimen. This spalling continued as long as the polymer was heated. Chemical analysis of the sand-like residue showed that there had been virtually no pyrolysis. There was a small amount of very thin char on the surface of some of the chips, but it was too small to be measurable.

Both microscopic examination of the polymer and analysis of the thermal stress patterns expected in the polymer indicated that the primary

mode of failure in this material was mechanical fracture due to nonuniform thermal stress gradients.

An analysis of typical thermomechanical properties of this type of polymer indicated that a thermal gradiant as small as 10°C/mm could cause cracking. As was seen in Fig. 6, the measured thermal gradients in these high-density polymers can exceed 600°C/mm. Therefore, thermomechanical failure would be expected in any high-density polymer in which the glass-transition temperature is high enough so that the thermal stresses can build up to a sufficient magnitude to crack the polymer before the polymer softens enough so that it can relieve those stresses.

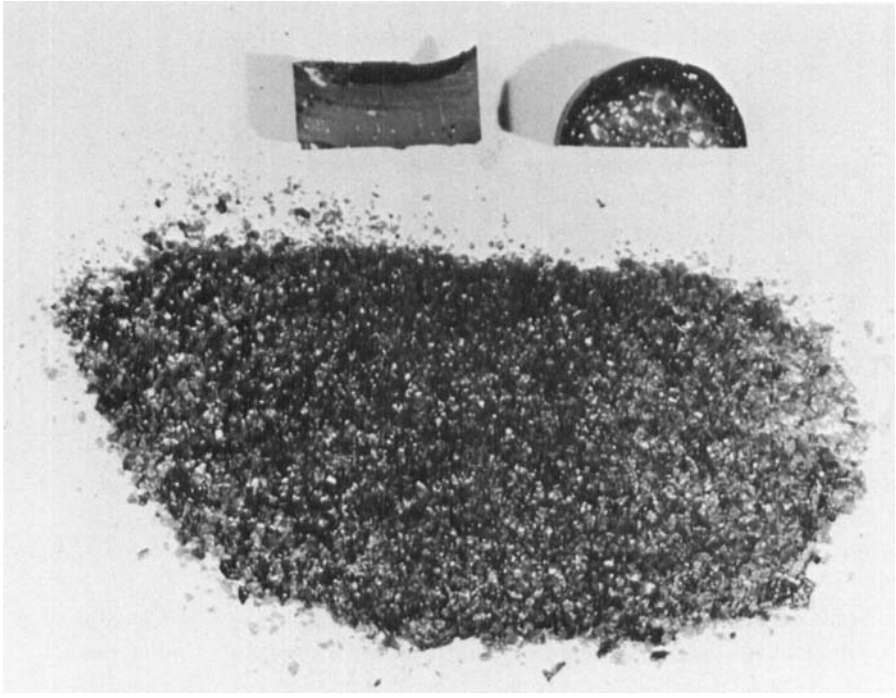

Fig. 12. Catastrophic failure of unreinforced epoxy polymer.

Once a crack has started, it tends to propagate because the reflective surfaces of the crack act as a light trap and cause further local heating and because of stress concentrations at the crack apex. These cracks will propagate until they reach a uniform temperature area or until a chip of polymer is cracked from the surface.

In the absence of any reinforcing agent, there would be nothing to prevent these chips from leaving the surface of the polymer with little or no charring. Figure 12 is an excellent example of this type of polymer failure.

However, the presence of only a small amount of the proper reinforcing material will prevent this type of failure. Photomicrographs of sectioned samples of an epoxy-novalac, DEN 438 reinforced with chopped quartz fiber, show vertical and horizontal cracks at the surface immediately adjacent to the char. These were caused by the thermal stress gradients generated in the polymer during pyrolysis. One picture showed a long rectangular surface chip, completely broken away from the polymer, which was prevented from leaving the surface by several silica fibers attaching it to the body of the polymer. This "anchoring" of chips of polymer is one of the major mechanisms by which reinforcing materials improve the properties of ablation materials.

A second role of reinforcement material appears to be reduction of the amount of surface cracking in proportion to the amount of fiber reinforcement. This is probably due to the quartz fiber decreasing the effective thermal expansion of the polymer and thus reducing the thermomechanical stresses.

In the high-density polymers the "yellow zone" is simply the area of cracked polymer just below the polymer-char interface. Chemical analysis of the polymer in this cracked area shows that it is essentially unreacted chemically. In addition, analyses of the measured temperature profiles within the polymer-char interface region indicate that this cracked area probably never exceeded 300°C.

The same cracking has been observed in the unreinforced high-density phenolic-nylon system as in the epoxy systems and in the epoxy-novalac systems. However, the unreinforced phenolic-nylon polymers are mechanically stable because the nylon in the cracked region has a low glass-transition temperature. In photomicrographs of the cracked zone, it can be seen that the nylon melts and cements the chips of polymer together until they have a chance to pyrolyze.

The second failure mode, shown in Fig. 13, occurs in the high-density epoxy-novalac polymer which has a low glass-transition temperature. Motion pictures were taken during the pyrolysis of this material and in these it is possible to see the polymer boiling. The boiling and frothing polymer chars in a very low-density state, and as a consequence, the char has a very low density. The chars formed from this material have the physical characteristics of cigar ash.

This polymer had very good characteristics during TGA testing.

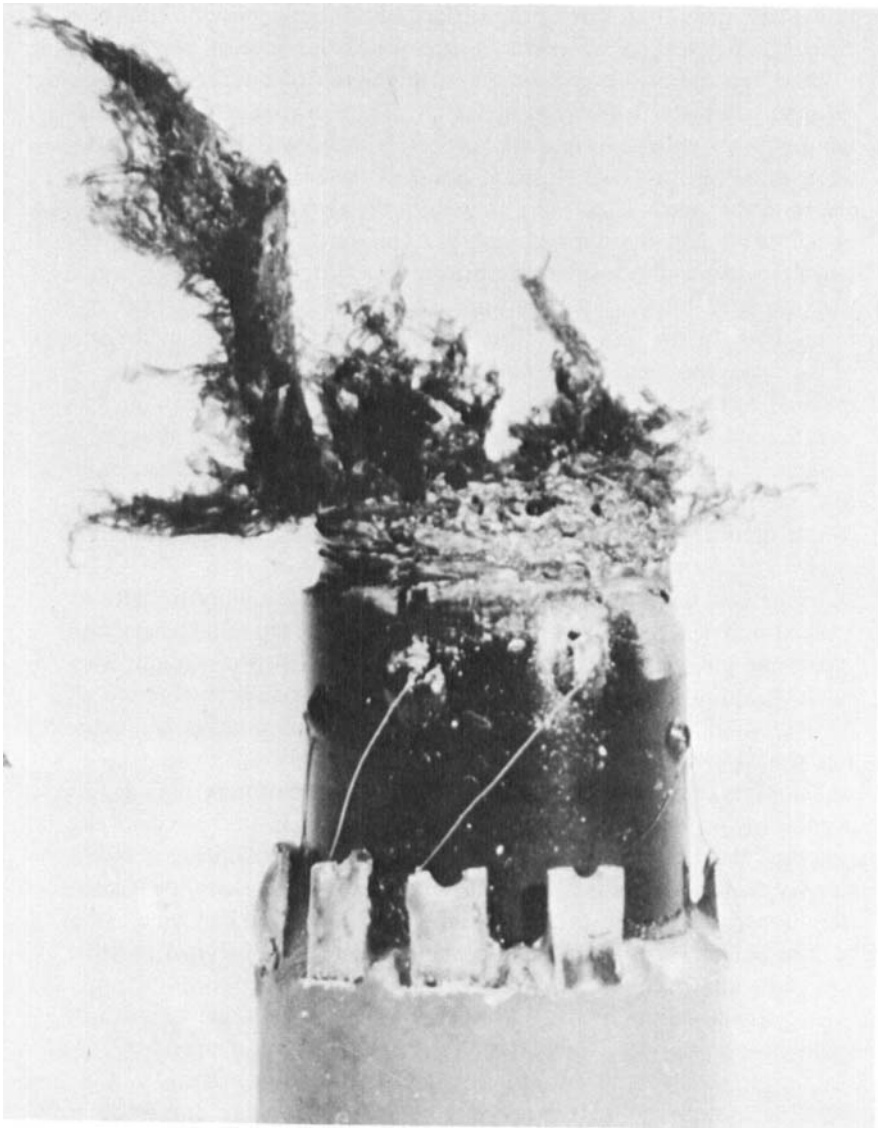

Fig. 13. Charring process in unreinforced DEN-438.

Therefore, a series of modifications of the pure polymer were undertaken in an attempt to control the thermophysical behavior of the polymer and make it usable as an ablation material. The most successful of these modifications was the addition of small amounts of chopped quartz fiber. Figure 14 is a photograph of the same polymer system shown in Fig. 13, but with 5 wt % quartz fiber added. This char was so tough that it could be removed from the polymer only by carving with a knife.

This dramatic change in char properties occurred because the quartz fiber was able to break the polymer foam and hold the liquid polymer in position so that it could char in a reasonably dense state. After the initial char formation had occurred, the quartz fibers bridged the liquid low-density gap between the char and the polymer and held the char cap on to allow additional pyrolysis to occur.

Figure 15 illustrates the periodic spalling failure mode. Materials that undergo this type of failure expel thin, uniform disks of char from their surfaces at regular intervals as long as they are exposed to the radiant flux. These disks are usually from 0.5 to 1.0 mm thick in the materials tested. The phenomenon has been observed in DEN-438 cresyl glycidyl ether with 5% milled quartz fibers and in DEN-438 with the following fillers: quartz microballoons, quartz microballoons with milled quartz fiber, and quartz microballoons with milled quartz fiber and carbon black. From the appearance of the chars, their thickness, and an examination of the quartz fibers (obtained by igniting polymer samples in air at 600°C), the mechanism of failure is readily apparent, as is discussed below.

It has been shown that for these types of materials there is a structurally weak, low-density zone about 0.7 mm wide between the primary pyrolysis zone and the char. In materials that show this periodic spalling-type failure, the measured length of the reinforcement fibers was around 0.25 to 0.35 mm, and these fibers were not long enough to bridge the low-density zone.

As the char formed, it was reinforced by the short fibers so that it formed a good strong char. However, as the char increased in thickness, the pressure drop of the pyrolysis gases passing through it increased. Eventually, a point was reached at which the gas pressure in the low-density zone exceeded the structural strength of that zone and the char cap was blown off. The process was repeated for as long as the sample was being heated.

To check this explanation, the fiber length of the chopped quartz fiber in a different sample of 5% quartz-filled DEN-438 was measured. In this material, which formed excellent chars of the kind shown in Fig. 14, the

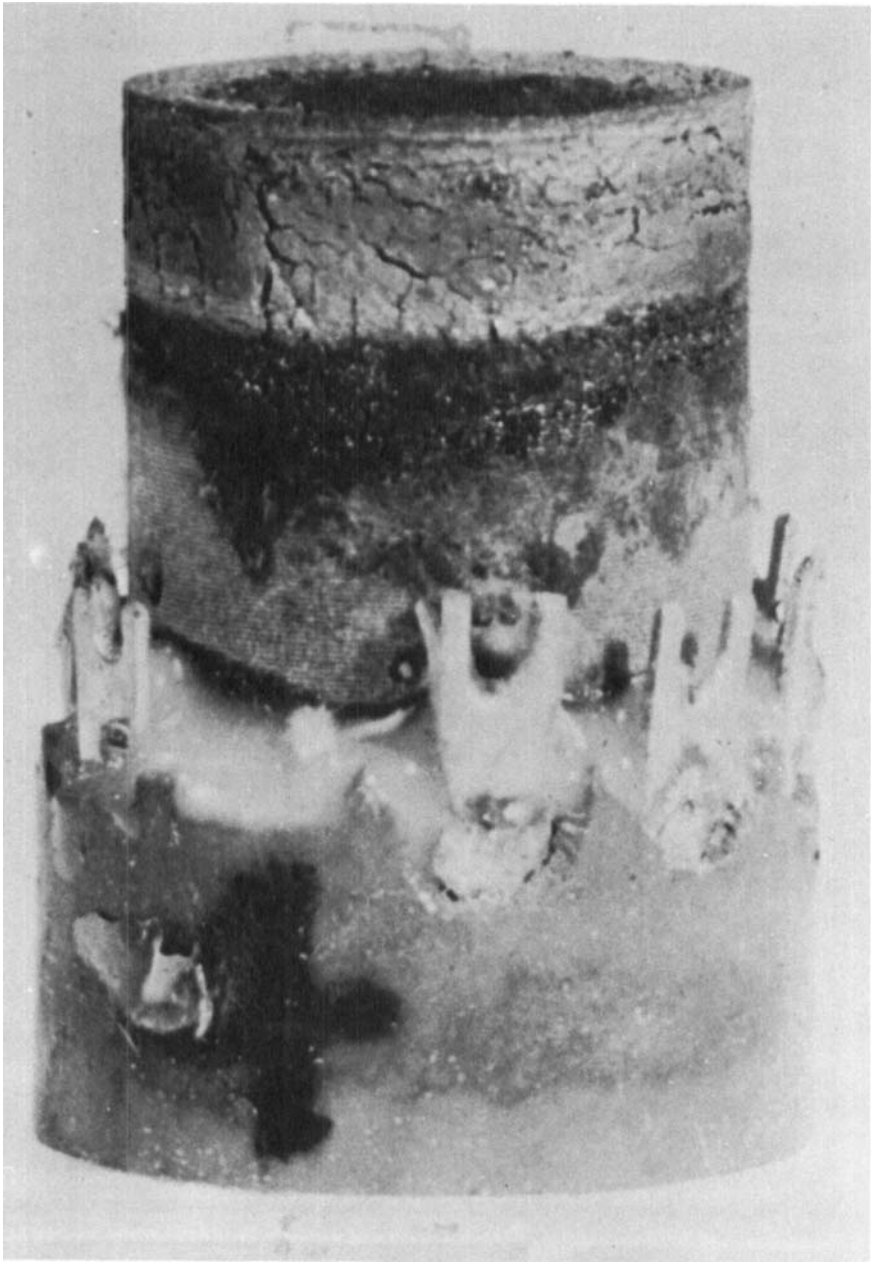

Fig. 14. Charring process in reinforced DEN-438.

fiber length was about 1.2 to 1.5 mm. Fibers of this length are capable of bridging the low-density zone and of acting as structural reinforcements to prevent the blow-off of char by pyrolysis-generated gas pressure.

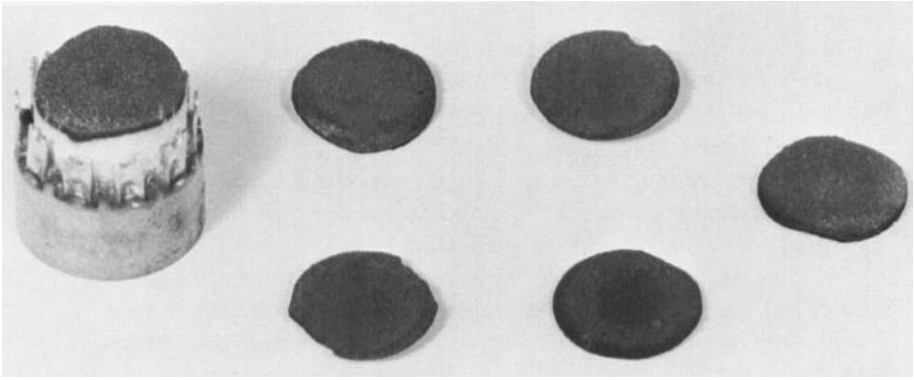

Fig. 15. Periodic spallation type of failure.

Therefore, from the examination of this type of failure mode, it is obvious that one of the major roles of the quartz fibers in reinforcing the high-density polymer systems is to bridge the low-density gap and provide an anchoring mechanism to hold the char onto the polymer. It therefore appears that the quartz fiber must always be of sufficient length to bridge the low-density, low-strength zone.

Another failure mechanism that was observed in motion pictures, taken during testing of polymers in the arc-image facility, was that of a structurally weak char due to the blowing of internally generated gas. During this type of failure, the gases generated at the polymer-char interface blow out through the char into the low-pressure region in front of the pyrolyzing sample. As the gases decrease in pressure going from the primary pyrolysis zone to the free gas space, they increase in velocity. Eventually, they reach sufficient velocity to aerodynamically shear the char near the front face of the specimen. This type of failure manifests itself by the formation of deep holes in the char in the region where the radiation is most intense. There is no evidence of melting of the char on examination after the run.

A series of experiments was performed to attempt to get an experimental value for the amount of sublimation that takes place during arc-image testing of these materials. The test material used was a

TGA-produced char from low-density phenolic nylon. The tests were completely unsuccessful, because immediately upon being exposed to the radiant heat flux the TGA char began to give off a very fine powder of char. This powdering continued as long as the char was exposed to the radiant heat flux.

To check the results of this test, a char was formed from a sample of low-density phenolic-nylon in the arc-image furnace. This char was removed from the polymer and was glued to a substrate of TGA char and then re-exposed to the arc-image flux.

The arc-image-produced char underwent no spalling or degradation of any sort, except for a very small amount of cratering at the focus of the arc-image light that was due to sublimation.

Microscopic examination of the two chars showed that there are significant differences in the appearance of these chars. The arc-image-produced char forms primarily as a system of columns of char that are normal to the char surface. If an arc-image char is broken it will cleave along the faces of these thin columns of char, whereas the TGA char will fracture randomly. It has also been observed that the arc-image char is considerably harder than the TGA-produced char. These results indicate that the physical properties measured on TGA-produced chars may be significantly different from those measured on chars produced under more realistic heating rate conditions.

CONCLUSIONS

Arc-image pyrolysis has been found to be a very useful technique for evaluating the thermophysical and thermochemical properties of ablation polymers. The following were the major findings of the study:

1. The front-surface temperature of an ablator char can undergo extremely rapid cooling (25-250°C/msec) if the heat flux is suddenly removed or changed. Thus, temperature measurements made on anything except a continuous basis can be seriously in error.

2. Measurements of the temperature profiles within pyrolyzing chars show that temperature changes of 400°C/sec and temperature gradients of 10,000°C/cm are not unusual.

3. Techniques were developed for analyzing the temperature data to determine the actual thermal diffusivity of the pyrolyzing system. This analysis showed that radiant heat transfer within the char is probably the dominant heat transfer mechanism above about 700°C. The mathematical

model was capable of correlating the measured data within a few per cent and of accurately predicting the internal temperature profiles and the rate of motion of isotherms within the pyrolyzing sample.

4. It was found that there was a very significant decrease in the rate of motion of the pyrolysis interface with increasing char thickness.

5. Analysis of the pyrolysis gases showed that during the first few seconds of pyrolysis high-molecular-weight vapors were produced but that after a char had formed the majority of the gases (90%) were CO and H_2.

6. Several independent sets of data proved that the pyrolysis occurs in essentially two steps: (a) Pyrolysis of the polymers to gaseous fragments occurs within about 0.5 mm of the front surface of the polymer, and (b) pyrolysis of the gaseous fragments to much lower-molecular-weight species, at about 1000°C, occurs in another 0.5 mm from the polymer surface.

7. Four different types of failure of polymer or polymer-char systems were isolated and explained. The addition of small amounts (less than 5%) of the proper length of quartz fiber eliminated all these failure modes.

REFERENCES

[1] H. S. Carslaw and J. C. Jaeger, *Conduction of Heat in Solids*, Clarendon, Oxford, 1948, p. 40.

[2] L. P. Kadanoff, *J. Heat Transfer*, **83**, 215-225 (1961).

[3] R. G. Nagler, *Tech. Rep. 32-1010*, Jet Propulsion Laboratory, February 1, 1967.

[4] G. R. Cunnington, F. J. Smith, and W. Bradshaw, *Paper No. 65-644*, Am. Inst. Aeron. Astronautics, Thermophys. Specialists Conf., Monterey, Calif., September 13–15, 1965.

[5] J. C. Chem and S. W. Churchill, *Am. Inst. Chem. Eng. J.*, **9**, 35-41 (1963).

Accepted by editor December 24, 1968
Received for publication January 3, 1969